Core-Shell Magnetic Fe_3O_4/CNC@MOF Composites with Peroxidase-Like Activity for Colorimetric Detection of Phenol

Chen Hou (houchen@sust.edu.cn)
Shaanxi University of Science and Technology Xi'an Campus: Shaanxi University of Science and Technology https://orcid.org/0000-0003-0981-672X

Linhui Fu
Shaanxi University of Science and Technology

Yang Wang
Shaanxi University of Science and Technology

Wenqiang Chen
Shaanxi University of Science and Technology

Fang Chen
Shaanxi University of Science and Technology

Sufeng Zhang
Shaanxi University of Science and Technology

Jianzhi Wang
Shaanxi University of Science and Technology

Research Article

Keywords: Cellulose nanocrystals, Metal organic framework, Mimic enzyme, Colorimetric detection, Phenol,

Posted Date: June 29th, 2021

DOI: https://doi.org/10.21203/rs.3.rs-645843/v1

Version of Record: A version of this preprint was published at Cellulose on August 7th, 2021. See the published version at https://doi.org/10.1007/s10570-021-04117-w.

Abstract

Rapid and accurate detection of phenolic wastewater from industries has created global concern. Herein, core-shell magnetic cellulose nanocrystals supported MOF (Fe_3O_4/CNC@ZIF-8) with robust peroxidase-like activity was synthesized with tannic acid as modifier and bridge. The peroxidase-mimic catalytic activity of as-prepared Fe_3O_4/CNC@ZIF-8 was further investigated using o-phenylenediamine (OPD) as peroxidase substrates in the presence of H_2O_2. Moreover, the experimental conditions were optimized and the kinetic analysis results showed that Fe_3O_4/CNC@ZIF-8 had higher affinity towards both the substrate OPD and H_2O_2 than horseradish peroxidase (HRP). Finally, a phenol colorimetric assay with a linear range of 2-200 μM and a detection limit of 0.316 μM was constructed. The catalytic mechanism of Fe_3O_4/CNC@ZIF-8 with phenol was further investigated by fluorescence test and the generated •OH was proved to act a crucial role to produce quinoid radicals. Additionally, the synthesized magnetic material had excellent stability and recyclability and ease to separation. These results suggest that the Fe_3O_4/CNC@ZIF-8 may be one of the promising candidates as peroxidase mimic for colorimetric detection of phenol.

Introduction

Numerous toxic pollutants are accumulated in the environment with the intensification of human activities and the acceleration of industrialization, which resulting in acute environmental problems and harm to human health. As one of the environmental contaminants, phenolic compounds have been widely applied in metallurgy, papermaking and chemical industry because they are important industrial raw materials(Niu et al. 2021). Wastewater containing phenol has the characteristics of tremendous harm and is detrimental to human health and the natural growth of aquatic organisms even the concentration is low(Mei et al. 2015). So far, various traditional analytical methods have been developed as means of phenol detection, such as chromatographic analysis(Arce et al. 2018), gas chromatography-mass spectrometry (GC-MS)(Meng et al. 2011), high performance liquid chromatography (HPLC)(Chen et al. 2013), fluorometry(Mitra and Saha 2016) and electrochemical analysis(Karimi-Maleh et al. 2014), etc. Although these methods have high sensitivity, disadvantages also have been revealed including complicated sample pretreatment procedures, expensive equipment and long-time to analysis. Colorimetric detection is a qualitative and semi-quantitative analysis of the target object based on color change, which does not need expensive equipment and can achieve on-spot detection(Wu et al. 2020). It has a great application prospect in the analysis of environmental pollutants and the process of medical care.

Phenol colorimetric detection is based on the catalytic reaction of the phenol with 4-aminoantipyrine (4-AAP) in the presence of the oxidant agent, forming pink color product through the naked eye observation (Zeng et al. 2015). Enzyme-mimics with nano-micron scale materials have been considered to facilitate the chromogenic reaction due to their high reactivity and multi-size effect. With the exploration of Fe_3O_4 nanoparticles (NPs) as mimetic peroxidase(Gao et al. 2007), various nanomaterials with enzyme-like

activity have been developed to possess superior catalytic specificity, activity and stability. Notably, metal organic framework (MOF) possess adjustable pore diameter, high specific surface area and exposed metal sites, showing strong peroxidase-like activity(Wu et al. 2017). For instance, MOF-808 was reported to be a novel peroxidase-like catalyst for glucose colorimetric biosensing at neutral pH(Zheng et al. 2018). The inherent problems of MOF powders arising from difficult separation could be overcome by using magnetic nanoparticles. Encapsulating Fe_3O_4 NPs in MOF to form a core-shell structure can easily separate the catalyst from the reaction system by an extra magnet with enhanced catalytic activity. However, the urgent problem of most magnetic nanoparticles is that they tend to be highly aggregated because of the large interaction of magnetic dipole(Ye et al. 2012).

To avoid the above problems, the stable support and surface modification become necessary. Cellulose nanocrystal (CNC), a low-cost and environmental friendly biomass material, has gained great interest as a stable support for nanoparticles immobilization due to its excellent biocompatibility, large aspect ratio and specific surface area(Batmaz et al. 2014). Moreover, the abundant hydroxyl groups on the surface of CNC can offer nucleating sites for the growth of nanoparticles(Low et al. 2018). Guo et al. have successfully synthesized amino-functionalized Fe_3O_4@CNC hybrids to further complex with Cu (II) ions to provide specific protein binding sites(Guo et al. 2017). Galland' group prepared cellulose nanofibers decorated with magnetic ferrite nanoparticles, which resulted in a rather uniform particle distribution due to the presence of cellulose nanofibers(Galland et al. 2013). Thus, constructing a colorimetric detection platform based on magnetic cellulose nanocrystal/MOF composites will be expected to be a novel material of great potential for the efficient detection of phenol.

With this in mind, we designed a core-shell magnetic Fe_3O_4/CNC@MOF nanocomposite as enzyme-mimic colorimetric sensor and applied for phenol detection. Tannic acid (TA) was utilized as adhesive agent to link Fe_3O_4/CNC and ZIF-8 NPs. The catechol and galloyl groups of TA are well known to bind with metal ions with high affinity to form metal-phenolic networks(Hao et al. 2020). Using magnetic Fe_3O_4/CNC as the supporter for MOF-based enzyme mimics colorimetric sensor is conducive to fast separation and alleviate aggregation of MOF nanoparticles. As designed, the Fe_3O_4/CNC@ZIF-8 nanocomposite exhibited intrinsic peroxidase-like activity and showed sharp color change upon adding to phenol solution. This work demonstrated convenient and effective phenol detection method upon cellulose-based enzyme mimic composites.

Experimental Section

Chemicals and Materials

Cellulose nanocrystal (CNC) was purchased from Tianjin Haojia Cellulose Co., Ltd. (Tianjin, China). Ferric chloride hexahydrate ($FeCl_3 \cdot 6H_2O$), ammonium acetate (NH_4OAc), ethylene glycol (EG), phenol, o-phenylenediamine (OPD), $NaCH_2COOH$ (NaAc), CH_3COOH (HAc), H_2O_2 (30%), 4-aminoantipyrine (4-AAP), 2-methylimidazole ($C_4H_6N_2$), zinc nitrate ($Zn(NO_3)_2 \cdot 6H_2O$), Tannic acid (TA), Polyethylene glycol-6000

(PEG-6000) and polyvinylpyrrolidone-10,000 (PVP-10000) were purchased from KeLuo Fine Chemicals Co., Ltd. (China); other chemicals and reagents were obtained from Tianjing Chemical Reagent Company (China). All the reagents used were of analytical grade without further purification.

Preparation of tannic acid modified magnetic cellulose composite

Magnetic cellulose composite was prepared through the one-pot solvothermal method as follows. First, 2.0 g CNC was dispersed in 20 mL ethylene glycol by ultrasonication with vigorous stirring for 30 min at room temperature (RT). Then, 0.8 g $FeCl_3 \cdot 6H_2O$ and 2.0 g NH_4Ac were added to the CNC dispersion in sequence. Next, another 20 mL ethylene glycol containing 0.75 g PEG was added to the mixed solution and kept stirring for another 30 min to form a homogeneous yellow dispersion. After that, the mixture was transferred in a Teflon-lined autoclave and maintained at 200 ℃ for 11 h. After natural cooling, the product were collected with the help of a magnet and washed with deionized (DI) water and ethanol several times. Finally, the catalysts were dried in a vacuum at 60 ℃ for 4 h. For comparison, the Fe_3O_4 NPs were prepared by following the same steps as showed above in the absence of CNC.

For the tannic acid functionalized Fe_3O_4/CNC, 100 mg Fe_3O_4/CNC was suspended in 20 mL DI water including 60 mg TA under gentle stirring at RT for 1 h. Then, the composites were magnetically isolated by an external magnet to obtain TA modified Fe_3O_4/CNC (Fe_3O_4/CNC/TA). The product was washed with DI water and followed by ethanol five times, respectively. Finally, the resulting mixture was placed in a 60°C oven under vacuum for 4 h to evaporate ethanol.

Preparation of the Fe_3O_4/CNC@ZIF-8 composite

Utilizing the chelation of the TA and metal ions, Zeolite imidazole framework-8 (ZIF-8) was synthesized on the surface of Fe_3O_4/CNC/TA. Briefly, 0.148 g of 2-methylimidazole was dissolved in 10 mL of methanol to form a clear solution. Then 50 mg as-prepared Fe_3O_4/CNC/TA was added to the above solution and stirred under the ultrasonication for 45 min at RT. Afterwards, 0.410 g of zinc nitrate hexahydrate dissolving 10 mL methanol was added to the mixture at 50°C and stirred for another 2 h. The obtained products named Fe_3O_4/CNC@ZIF-8 were separated by a magnet and washed with water and methanol several times, subsequently dried under vacuum at 60°C for 4 h.

Characterization

Transmission electron microscopy (TEM) on a FEI Tecnal G^2F30 and scanning electron microscopy (SEM, Hitachi S-4800, Hitachi, Japan) with energydispersive X-ray spectroscopy (EDS) were used to characterize the microstructure and morphology of the sample. Samples crystal structure were obtained by The powder X-ray diffraction analysis (XRD Bruker, D8-Advance, Karlsruhe, Germany) with Cu Kα radiation (λ = 1.542 Å) at 10–80° (2θ). The chemical structure of composites was characterized by Fourier transform infrared (FT-IR, Bruker VERTEX 70, Karlsruhe, Germany) spectra with a wavelength range of 4000 to 400 cm^{-1}. Temperature-mass curve of the materials were tested by thermal gravimetric analysis (TG,

STA449F3-1053-M, Germany), which was carried out in nitrogen atmosphere with a heating rate of 10°C min^{-1} from 30 to 800°C. The specific surface area was calculated by the Bruner-Emmett-Teller (BET) method. The magnetic properties of the obtained magnetic composite materials were evaluated using a vibrating sample magnetometer VSM 7304 (Lakeshore, Columbus, OH, USA) at room temperature. The chemical state of the elements in the sample was characterized by X-ray photoelectron spectroscopy (XPS, AXIS SUPRA, UK). Fluorescence spectra were recorded on an RF-5301PC fluorescence spectrophotometer (Shimadzu Co., Ltd, Japan) equipped with a Xenon lamp to detect free radicals in the catalytic reactions. Colorimetric experiments were performed on The UV-Vis spectra (China, Shanghai, Shimadzu UV-2501 PC spectrometer).

Evaluation of the peroxidase-mimic catalytic activity of Fe_3O_4/CNC@ZIF-8

The peroxidase-like activity of the Fe_3O_4/CNC@ZIF-8 was investigated in the sensing of H_2O_2 by the oxidation reaction of a colorless substrate OPD to form the yellow product (2, 3-diaminophenazine, DAP) (Lin Z et al. 2014). In a typical experiment, 4 mg Fe_3O_4/CNC@ZIF-8, 500 µL 0.5 mM OPD and different concentration of H_2O_2 (0-200 µM) was added into 0.2 M NaAc-HAc buffer (pH 4.0) so as to make a total volume of 3.0 mL. Subsequently, the mixed solution incubated at RT for 20 min. UV-vis measurement was used to determine the obtained yellow-colored solution by monitoring the absorbance at the wavelength of 450 nm. The peroxidase-like activity of Fe_3O_4/CNC@ZIF-8 at different temperatures and pH values were also studied.

Kinetic analysis of Fe_3O_4/CNC@ZIF-8 peroxidase-like activity

Kinetic analysis was performed using steady state kinetics followed previous literature, which was conducted by changing the concentration of one substrate (OPD or H_2O_2) at fixing the other substrate(Yang et al. 2020). All experiments were carried out in 1.0 mL cuvettes with a path length (l) of 1.0 cm at RT. The Beer Lambert's law can change the absorbance value to their corresponding concentration:

$$A = \varepsilon \times c \times l \quad (1)$$

Where, A is the absorbance at 450 nm, ε is the molar absorptivity (= 1.67×10^4 M^{-1} cm^{-1} for DAP at 450 nm)(Vetr et al. 2018), c represents the concentration of one substrate.

For the kinetic determination of OPD, 8 mg Fe_3O_4/CNC@ZIF-8 was added to a NaAc-HAc buffer (0.2 M pH 4.0) containing different concentrations of OPD (0.125–1.25 mM) in the presence of 70 µM H_2O_2 with a total volume of 3.0 mL. The absorbance at 450 nm was immediately recorded at a 60 s interval within 10 min. As a comparison, the kinetic determination of H_2O_2 was carried out by fixing the concentration of OPD (0.5 mM) and varying the H_2O_2 concentration (10–80 µM). Then the "absorbance *vs* time" plots were obtained to calculate the initial point ($Slope_{initial}$) of each curve. The initial reaction velocity (v) was

calculated with the formula: $Slope_{initial}$ / (ε × l). All of the v against substrate concentrations ([S]) plots were then fitted via nonlinear regression of the Michaelis-Menten equation. Finally, the Michaelis constant (K_m) was obtained from the Lineweaver-Burk double reciprocal plot generated from the Michaelis-Menten equation, where V_{max} is the maximal reaction velocity:

$$\frac{1}{v} = \frac{K_m}{v_{max}} \times \frac{1}{[S]} \times \frac{1}{v_{max}} \quad (2)$$

Colorimetric detection of phenol

For phenol detection, a chromogenic reaction based on the oxidative coupling between the phenol and 4-AAP in the presence of the H_2O_2 was conducted at RT. Briefly, 800 µL 4-AAP (80 mM), 900 µL H_2O_2 (110 mM) and different concentration of phenol (0-200 µM) were added into NaAc-HAc buffer (0.2 M pH 4.0). Then, 4 mg Fe_3O_4/CNC@ZIF-8 was rapidly added, and the mixture incubated for 20 min at RT until a pink mixture was obtained. The mixture was separated through external magnet to remove the precipitate, and the absorbance of the supernatant was monitored by UV-vis spectrophotometer at the wavelength of 525 nm. All the measurements were carried out in triplicate and the results from the obtained parallel data were averaged.

In addition, the selectivity of Fe_3O_4/CNC@ZIF-8 toward phenol was investigated. Aqueous solutions of different interfering substances in DI water, such as acetone, ethanol, ethyl ether, imidazole, benzene, cyclohexane and sodium sulfite, were prepared and similarly tested under the same experimental conditions.

Results And Discussion

Synthesis and characterization of Fe_3O_4/CNC@ZIF-8

SEM and TEM images were used to characterize to study the surface morphology and particle size of the Fe_3O_4/CNC and Fe_3O_4/CNC@ZIF-8 (Fig. 1). The rod-like structures of CNC can interweave each other to form a web-like network, which was a good support to prevent the aggregation of Fe_3O_4 NPs(An et al. 2017). SEM image of Fe_3O_4/CNC showed that Fe_3O_4 NPs loading on CNC had a nearly spherical morphology with a rough surface, and particle size ranged between 100 and 250 nm(Fig. 1(a)). TEM micrograph (Fig. 1(b)) evidenced that Fe_3O_4 NPs were well dispersed in the CNC network after solvothermal process. In Fig. 1(c), thin tannic acid shell layers had formed around the Fe_3O_4/CNC cores, which were utilized as the adhesive coating on the surface of Fe_3O_4/CNC to guarantee a homogeneous growth of ZIF-8. As seen from Fig. 1(d) and Fig. 1(e), SEM image of Fe_3O_4/CNC@ZIF-8 confirmed that the Fe_3O_4/CNC was successfully coated with ZIF-8 to form Fe_3O_4/CNC@ZIF-8 complex, and ZIF-8 exhibited a cubic crystal structure. Compared with the TEM image of Fe_3O_4/CNC, Fe_3O_4/CNC@ZIF-8

nanocomposites exhibited a distinct core-shell structure, and the average size of ZIF-8 shell was approximately 40 nm. Under a higher magnification of TEM, continuous and uniform ZIF-8 NPs were well incorporated on the Fe_3O_4/CNC surface (Fig. 1(f)), demonstrating the successful synthesis of Fe_3O_4/CNC@ZIF-8. Furthermore, Energy-dispersive X-ray spectroscopy (EDS) of Fe_3O_4/CNC@ZIF-8 was shown (Fig. S1), and the presence of Fe, O, N and Zn as expected to be observed in Fe_3O_4/CNC@ZIF-8.

The FT-IR spectra were illustrated in Fig. 2(a) to contrast the functional groups on Fe_3O_4, ZIF-8 and Fe_3O_4/CNC@ZIF-8 surface. Concretely, for pure CNC, the peaks at 1060 and 2904 cm^{-1} were caused by the C-O-C stretching of pyranose and the C-H stretching vibration, respectively(Xiong et al. 2013). The broad peak in the band of 3464 cm^{-1} corresponded to the O-H stretching vibration, while the absorbance band at 1609 cm^{-1} originated from O-H bending vibration(Jahan et al. 2010). In the case of Fe_3O_4/CNC, the peak derived from Fe-O bonds was expected at 582 cm^{-1}, indicating that the Fe_3O_4 NPs were successfully immobilized on the CNC. O-H stretching of CNC became weak due to the interactions of the hydroxyl groups and Fe_3O_4 NPs(Liu et al. 2015). The spectrum of Fe_3O_4/CNC after TA coating displayed some changes including the -OH stretching of the phenolic and methylol group that appeared at 3420 cm^{-1}. Additionally, the 1718 and 1080 cm^{-1} vibrational bands corresponded to the C = O and C-O stretching vibrations, respectively. The peaks at 1434 and 1346 cm^{-1} in the spectrum of TA belonged to the aromatic C-C and phenolic C-O stretching vibrations, respectively(Dutta and Dolui 2011). Moreover, One-layer coating TA-CNC was also obtained due to the hydrogen bonding between TA and the C6 hydroxyl group of the CNC. For the Fe_3O_4/CNC@ZIF-8, the significant observed bands around 3136 and 2928 cm^{-1} were ascribed to the stretching vibration of C-H in methyl and imidazole rings. Worthwhile mentioning that the series of complex and compact observed bands in the spectra of 700–1350 cm^{-1} and 1350–1500 cm^{-1} can be attributed to the stretching and plane bending of imidazole ring(Zheng et al. 2014). The absorption peaks at 421 and 759 cm^{-1} were ascribed to the nature of the ZIF-8 structure confirming the formation of the Zn-N bond.

The XRD patterns for the different samples were shown in Fig. 2(b). The broad and strong peaks at 14.9° and 24.5° were assigned to the (110) and (002) planes of CNC, respectively(French 2013). Besides, Fe_3O_4/CNC exhibited similar diffraction peaks with Fe_3O_4 NPs at 19.90°, 30.59°, 36.01°, 43.50°, 57.2°, and 62.8°, which corresponded to the (220), (311), (222), (400), (422), (511), and (440) lattice planes. These results further indicated the successful synthesis of Fe_3O_4 in the CNC. After loading of the ZIF-8, the XRD patterns showed new diffraction peaks at 2θ = 7.2° (011), 10.3° (002), 12.6° (112), 14.7° (022), 16.6° (013), 17.8° (222), 24.5° (233) and 26.7° (134) (JCPDS card No. 89-3739 for ZIF-8), highlighting the ZIF-8 was successfully coated on the Fe_3O_4/CNC. XRD analysis revealed the favorable crystalline structure of Fe_3O_4/CNC@ZIF-8.

N_2 adsorption-desorption isotherms of Fe_3O_4/CNC@ZIF-8 was shown in Fig. 3(a)), and the isotherm of nanocomposites displayed a typical type IV isotherm. The pore width was 5.1 nm and the BJH pore volume was 0.31cm^3/g, indicating a typical mesoporous structure. The BET surface area of

Fe_3O_4/CNC@ZIF-8 was 463.63 m^2/g, which was larger than many detection materials (Table S1). These analyses suggested that Fe_3O_4/CNC@ZIF-8 possessed a high surface area and mesoporous structure, which would probably provide more active sites and thereby improve the catalytic activity. Additionally, the hysteresis curve of sample magnetization were tested by VSM instrument and the result was shown in Fig. 3(b). The saturation magnetization (M_s) value of Fe_3O_4 was about 79.11 emu/g. In contrast with Fe_3O_4, the relatively weak magnetism Fe_3O_4/CNC (59.65 emu/g) and Fe_3O_4/CNC@ZIF-8 (44.01 emu/g) were mainly due to the TA coating and dielectric property of the outer shell. Nevertheless, the Fe_3O_4/CNC@ZIF-8 still held strong magnetism and responded rapidly to external magnetic field, which was conveniently separated in the post-treatment process of wastewater.

XPS analysis was further performed to investigate the element composition and the chemical states of the Fe_3O_4/CNC@ZIF-8. The XPS spectrum showed the surface composition of Fe_3O_4/CNC@ZIF-8 containing C, N, O, Fe and Zn elements as seen in Fig. 4(a). The binding energy of 285.5 eV was related to C-C in cellulose, which indicated the successful synthesis of Fe_3O_4/CNC(Hu et al. 2017). Additionally, the peaks at 398.8 eV in Fig. 4(a) represented N 1s, supporting the presence of the C = N–C in the ZIF-8(Yang et al. 2015). To amply reveal the microscopic interactions, the C 1s XPS spectrum was shown in Fig. 4(b) and three peaks at 284.04, 284.65 and 285.2 eV were associated with C-C, C = N and C-N, respectively(Chen et al. 2021). For O 1s in Fig. 4(c), the peak appeared at 531.91, 532.53 and 533.72 eV were in line with -OH, N-O and -COOH. One small Zn 2p peak observed at 1021.45 eV was assigned to zinc (+ 2) oxide, and the spectra of Zn 2p were in good agreement with its oxidation state. On the basis of previous work, the two characteristic peaks locating at 1021.8 and 1044.8 eV in the high resolution spectrum of Zn were due to Zn $2p_{3/2}$ and Zn $2p_{1/2}$, respectively, further indicating the presence of ZIF-8 (Fig. S2)(Yang et al. 2015). Notably, the Fe 2p spectrum showed the main peaks at around 710.7 and 724.2 eV mainly corresponded to the $Fe2p_{3/2}$ and $Fe2p_{1/2}$, respectively, obviously demonstrating the existence of Fe_3O_4 (Fig. 4(d))(Wu et al. 2019).

Peroxidase-like activity of Fe_3O_4/CNC@ZIF-8 and the detection of H_2O_2

The peroxidase-like activity of ZIF-8, Fe_3O_4/CNC and Fe_3O_4/CNC@ZIF-8 were studied at room temperature and the formation of the typical yellow product (2, 3-diaminophenazine, DPA) with a maximum adsorption at 450 nm was monitored by UV-vis absorption. In Fig. 5(a), the UV-vis absorption spectra at 450 nm were observed for ZIF-8, Fe_3O_4/CNC and Fe_3O_4/CNC@ZIF-8 systems and the absorption intensity of Fe_3O_4/CNC@ZIF-8 was comparatively high to ZIF-8 and Fe_3O_4/CNC. The inserted photographic image showed the color change of the different catalytic systems. It was observed that the mixed solution of OPD with either H_2O_2 or Fe_3O_4/CNC@ZIF-8 was colorless or slight yellow. Both the UV-vis absorption spectra and the naked eye detection demonstrated that the Fe_3O_4/CNC@ZIF-8 had excellent peroxidase-like catalytic ability to effectively catalyze the OPD oxidation. The reason behind this was that the interlaced web-like network structures of CNC can enhance the dispersion of Fe_3O_4 NPs.

Besides, ZIF-8 possesses a porous structure with a large number of exposed active sites, which coated on the surface of Fe_3O_4 NPs to further improve the peroxidase-like activity of the composite.

It is known that the peroxidase-like catalytic activity of Fe_3O_4/CNC@ZIF-8 nanocomposites depends on the pH values, temperature and catalyst dosage. Therefore, the catalytic activity of Fe_3O_4/CNC@ZIF-8 was investigated in detail through modulating these factors. In Fig. S3(a), with the catalyst dosage increased from 2 to 12 mg, the catalytic activity first rose and then gradually fell, exhibiting the optimum catalyst dosage at 8 mg. Moreover, the pH and temperature were important factors affecting the performance of peroxidase catalysts, and hence various pH from 2.0 to 6.0 and temperature from 20 to 60 ℃ were studied (Fig. S3(b) and (c)). The catalytic activity achieved a higher level in acidic solutions (pH 3.5–4.5) than in strong acidic or alkaline solutions. The maximum catalytic activity was obtained in a solution at pH 4.0 similar to HRP(Qiao et al. 2014). In addition, Fe_3O_4/CNC@ZIF-8 exhibited quite commendable catalytic activity even the temperature at 55 ℃, indicating the catalytic possessed a good temperature resistance.

Under the optimal conditions, the Fe_3O_4/CNC@ZIF-8 was used for the sensitive assay of H_2O_2 by colorimetry. The UV-vis spectra of the different concentration of H_2O_2 were displayed in Fig. 5(b), which observed the absorbance increased gradually with the increasing of H_2O_2 concentration at 450 nm. Figure 5(c) showed a good linear relationship (R^2 = 0.9954) between absorbance value and H_2O_2 concentration in the range from 2 to 200 μM with a limit of detection (LOD) of 2.24×10^{-7} M (S/N = 3). Correspondingly, a clear color change from colorless to dark yellow was obviously differentiated by the naked eyes shown in Fig. 5(d). These results showed that the Fe_3O_4/CNC@ZIF-8 has great potential in the quantitative analysis of H_2O_2 detection.

Detection of phenol and optimization of reaction conditions

As expected, a colorimetric detection method of phenol had been established, which was proven a high-throughput analytical method with fast and visual readout advantages. When phenol is present, it can be oxidized by the Fe_3O_4/CNC@ZIF-8 forming the pink-colored complexes in the presence of H_2O_2, exhibiting a characteristic absorption peak at 525 nm(Wu et al. 2020). As shown in Fig. 6 (a), the reaction system including Fe_3O_4/CNC@ZIF-8 and H_2O_2 (curve e) appeared obvious pink compared to that of the control experiment (curve a and b). Furthermore, in comparison with experimental system consisted of either Fe_3O_4/CNC@ZIF-8 or H_2O_2 (curve d and e), both of them existed in the system could enhance the color reaction and generate a strong absorption peak at 525 nm. These results indicated that Fe_3O_4/CNC@ZIF-8 possessed a higher catalytic activity in the presence of H_2O_2 than that of Fe_3O_4/CNC and pure ZIF-8.

Various experimental parameters were examined and optimized as follows to find the suitable conditions for phenol detection. Since the reaction used 4-AAP as a chromogenic agent in the presence of an oxidant agent to produce a colored compound, changes in 4-AAP and H_2O_2 concentrations directly affected the efficiency of reaction. The influence of the 4-AAP concentration was studied in the range of 2.0–10.0 mM

(Fig. S4 (a)), and the maximum absorbance was obtained with the 4-AAP concentration in 8.0 mM. As shown in Fig. S4 (b), an improvement in absorbance intensity was observed with the H_2O_2 concentrations increasing from 0.01 to 0.1 M and decreased slowly after that. Therefore, H_2O_2 concentration of 0.1 M was chosen for subsequent experiments. For temperature factor, the maximum catalytic activity for Fe_3O_4/CNC@ZIF-8 revealed that 50°C was the optimal incubation temperature Fig. S4 (c).

Figure 6 (b) demonstrated that when the phenol concentration was 0-200 μM, as the phenol concentration increased, the absorbance value gradually increased. A linear response was obtained between the absorbance and the phenol concentration in the range of 2-200 μM with the coefficient of correlation (R^2) equal to 0.9908 (Fig. 6 (c)). The LOD of the designed phenol analysis platform was 3.16×10^{-7} M (S/N = 3). Comparing the detection ranges and LODs of different materials for detecting phenol, it indicated that the Fe_3O_4/CNC@ZIF-8 material has certain advantages in phenol detection (Table S2).

Steady-state kinetic assay of Fe_3O_4/CNC@ZIF-8

Based on these optimal conditions, the Michaelis-Menten behavior of the Fe_3O_4/CNC@ZIF-8 was evaluated by steady-state kinetics analysis with H_2O_2 and OPD as substrates, respectively. The oxidation reaction process of Fe_3O_4/CNC@ZIF-8 followed the conventional enzymatic dynamic regulation of the Michaelis-Menten equation. In Fig. 7, the Lineweaver-Burk plots were used to calculate the steady-state kinetics fitting parameters of the Michaelis-Mentenconstant (K_m) and maximum initial velocity (V_{max}). As shown in Table 1, the K_m value of Fe_3O_4/CNC@ZIF-8 with OPD as substrate was 0.883 mM, two times lower than that of HRP (1.80 mM). It was confirmed that Fe_3O_4/CNC@ZIF-8 had a better affinity for OPD than HRP due to the large surface area of catalysts and good dispersion of Fe_3O_4 NPs coated with ZIF-8. The K_m value of Fe_3O_4/CNC@ZIF-8 with H_2O_2 was 0.171 mM, which was smaller than that of HRP (0.214 mM). It was indicated lower H_2O_2 concentration for Fe_3O_4/CNC@ZIF-8 could achieve maximum activity than that of HRP. Furthermore, the Fe_3O_4/CNC@ZIF-8 had a much smaller K_m and higher V_{max} than those of HRP(Kergaravat et al. 2012; Qiao et al. 2014), demonstrating that Fe_3O_4/CNC@ZIF-8 possessed higher activity and catalytic efficiency than that for HRP.

Table 1
Comparison of kinetic parameters of Fe_3O_4/CNC@ZIF-8 and HRP

Catalyst	Substance	K_m (mM)	V_{max} ($MS^{-1}\times10^{-8}$)
Fe_3O_4/CNC@ZIF-8	H_2O_2	0.171	0.893
Fe_3O_4/CNC@ZIF-8	OPD	0.883	0.524
HRP	H_2O_2	0.214	0.246
HRP	OPD	1.800	0.120

To gain a better understanding of the mechanism towards the reaction of phenol and 4-AAP to form a pink quinone imine, p-phthalic acid (PTA) was chosen as a fluorescence probe. Terephthalic acid can react with •OH to produce a fluorescent product 2-hydroxy terephthalic acid (HTA), which can be observed through fluorescence spectroscopy by displaying a fluorescent emission peak at 410 nm(Barreto 1994). In detail, 4 mg Fe_3O_4/CNC@ZIF-8 was firstly added to the mixture containing 100 µL 0.1 M H_2O_2, 2.89 mL NaAc-HAc buffer (0.2 M pH 4.0) for reaction. Then, 10 µL 5 mM terephthalic acid solution was added to the above solution. Subsequently, the mixed solution incubated for 20 min at room temperature, and the fluorescence spectrum was recorded with an excitation wavelength at 325 nm. As illustrated in Fig. 8(a), both PTA and PTA + Fe_3O_4/CNC@ZIF-8 system showed almost no fluorescence at 325 nm, while Fe_3O_4/CNC@ZIF-8 + H_2O_2 + PTA system had strong fluorescence intensity, confirming that Fe_3O_4/CNC@ZIF-8 can catalyze H_2O_2 to produce •OH during the peroxidase-like reaction. The reaction mechanism was clearly illustrated in Fig. 8(b). Fe_3O_4/CNC@ZIF-8 + H_2O_2 + PTA played the peroxidase-like catalytic activity and catalyzed H_2O_2 to produce •OH. Subsequently, the •OH with strong oxidizing capacity induce phenol to generate the quinoid radicals, which then reacted with 4-AAP in the presence of redundant •OH to form a pink quinone imine(Wu et al. 2020).

Selectivity and reusability of Fe_3O_4/CNC@ZIF-8

Selectivity is significantly important to establish excellent colorimetric assay. Control experiments were carried out under the same condition in the presence of phenol and other coexisting substances. The changes of absorbance at 505 nm were monitored by UV-vis spectrophotometer, and the experimental results were exhibited in Fig. 9(a), almost no apparent absorbance at 525 nm along with slight color change were observed in the reaction solutions with interfering substances. However, the reaction solution revealed a remarkable color variation from colorless to pink accompanied with a strong absorbance at 525 nm.

In addition, the reusability of the synthesized Fe_3O_4/CNC@ZIF-8 was investigated by cyclic experiments. UV-vis spectrophotometer was used to record the absorbance of the reaction systems at 525 nm. After each cycle, the composite was separated from the reaction system with extra magnet, and washed by DI water and ethanol five times and dried, which was reused for the next cycle. In Fig. 9(b), the absorbance

values of the reaction system had negligible change after sextic tests. Therefore, these results further confirmed the excellent selectivity and reusability of Fe_3O_4/CNC@ZIF-8-based phenol assay platform, offering a feasible and promising strategy for detecting phenol simple, rapidly and sensitively in actual samples.

Conclusion

In summary, Fe_3O_4/CNC@ZIF-8 nanocomposites as a novel peroxidase mimic were successfully synthesized by simple one-step solvothermal and in-situ growth method. The as-prepared Fe_3O_4/CNC@ZIF-8 was demonstrated to possess outstanding intrinsic peroxidase-like activity compared to the Fe_3O_4/CNC and ZIF-8. Furthermore, the steady-state kinetic parameters (K_m and V_{max}) also theoretically proved Fe_3O_4/CNC@ZIF-8 nanocomposites had stronger affinity for OPD and a fast catalytic rate. Characterization analyses found that the Fe_3O_4/CNC@ZIF-8 exhibited superior catalytic activity due to the unique core-shell structure and well-dispersed nanoparticles on the CNC. On the basis of the intrinsic peroxidase-like activities, a simple colorimetric sensing system of phenol was constructed and 0.316 μM of the LOD was obtained in the linear range of 2-200 μM. The Fe_3O_4/CNC@ZIF-8 was magnetically separable along with the recycled up to 6 times and the detection mechanism was probed by fluorescence spectroscopy. Consequently, owing to rapid response, low cost, as well as robust catalytic properties, Fe_3O_4/CNC@ZIF-8 nanocomposites are competent to an excellent peroxidase mimics catalysts for colorimetric detection of phenol in environmental monitoring.

Declarations

Acknowledgments This work was supported by the National Natural Science Foundation of China (No. 21806096), the China Postdoctoral Science Foundation (2020M683412), the Natural Science Basic Research Plan in Shaanxi Province (2021JQ-529) and the Special Research Program of Shaanxi Provincial Department of Education (20JK0541)

Availability of data and material My research didn't generate any data or I reused existing data.

Compliance with Ethical Standards

Conflict of interest We declare that we do not have any commercial or associative interest that represents a conflict of interest in connection with the work submitted.

Research involving human participants and/or animals

We have no research involving human participants and/or animals

References

1. An X, Long Y, Ni Y (2017) Cellulose nanocrystal/hexadecyltrimethylammonium bromide/silver nanoparticle composite as a catalyst for reduction of 4-nitrophenol. Carbohydr Polym 156:253-258. https://doi.org/10.1016/j.carbpol.2016.08.099
2. Arce MM, Sanllorente S, Ortiz MC, Sarabia LA (2018) Easy-to-use procedure to optimise a chromatographic method. Application in the determination of bisphenol-A and phenol in toys by means of liquid chromatography with fluorescence detection. J Chromatogr A 1534:93-100. https://doi.org/10.1016/j.chroma.2017.12.049
3. Barreto JC, Smith, GS, Strobel, N, Mcquillin, PA, Miller, TA. (1994) Terephthalic acid: a dosimeter for the detection of hydroxyl radicals in vitro. Life Sci 56:89-96. https://doi.org/10.1016/0024-3205(94)00925-2
4. Batmaz R, Mohammed N, Zaman M, Minhas G, Berry RM, Tam KC (2014) Cellulose nanocrystals as promising adsorbents for the removal of cationic dyes. Cellulose 21:1655-1665. https://doi.org/10.1007/s10570-014-0168-8
5. Chen B, Huang Y, He M, Hu B (2013) Hollow fiber liquid-liquid-liquid microextraction combined with high performance liquid chromatography-ultraviolet detection for the determination of various environmental estrogens in environmental and biological samples. J Chromatogr A 1305:17-26. https://doi.org/10.1016/j.chroma.2013.06.029
6. Chen M, Wang N, Wang X, Zhou Y, Zhu L (2021) Enhanced degradation of tetrabromobisphenol A by magnetic Fe_3O_4@ZIF-67 composites as a heterogeneous Fenton-like catalyst. Chemical Engineering Journal 413. https://doi.org/10.1016/j.cej.2020.127539
7. Dutta A, Dolui SK (2011) Tannic acid assisted one step synthesis route for stable colloidal dispersion of nickel nanostructures. Appl Surf Sci 257:6889-6896. https://doi.org/10.1016/j.apsusc.2011.03.025
8. French AD (2013) Idealized powder diffraction patterns for cellulose polymorphs. Cellulose 21:885-896. https://doi.org/10.1007/s10570-013-0030-4
9. Galland S, Andersson RL, Salajková M, Ström V, Olsson RT, Berglund LA (2013) Cellulose nanofibers decorated with magnetic nanoparticles-synthesis, structure and use in magnetized high toughness membranes for a prototype loudspeaker. Journal Mater Chem C 1:7963. https://doi.org/10.1039/c3tc31748j
10. Gao L et al. (2007) Intrinsic peroxidase-like activity of ferromagnetic nanoparticles. Nat Nanotechnol 2:577-583. https://doi.org/10.1038/nnano.2007.260
11. Guo J et al. (2017) Complexes of Magnetic Nanoparticles with Cellulose Nanocrystals as Regenerable, Highly Efficient, and Selective Platform for Protein Separation. Biomacromolecules 18:898-905. https://doi.org/10.1021/acs.biomac.6b01778
12. Hao S, Shao C, Meng L, Cui C, Xu F, Yang J (2020) Tannic Acid-Silver Dual Catalysis Induced Rapid Polymerization of Conductive Hydrogel Sensors with Excellent Stretchability, Self-Adhesion, and Strain-Sensitivity Properties. ACS Appl Mater Inter 12:56509-56521. https://doi.org/10.1021/acsami.0c18250

13. Hu Z, Meng Q, Liu R, Fu S, Lucia LA (2017) Physical Study of the Primary and Secondary Photothermal Events in Gold/Cellulose Nanocrystals (AuNP/CNC) Nanocomposites Embedded in PVA Matrices. ACS Sustain Chem Eng 5:1601-1609. https://doi.org/10.1021/acssuschemeng.6b02380
14. Jahan MS, Saeed A, He Z, Ni Y (2010) Jute as raw material for the preparation of microcrystalline cellulose. Cellulose 18:451-459. https://doi.org/10.1007/s10570-010-9481-z
15. Karimi-Maleh H, Moazampour M, Ensafi AA, Mallakpour S, Hatami M (2014) An electrochemical nanocomposite modified carbon paste electrode as a sensor for simultaneous determination of hydrazine and phenol in water and wastewater samples. Environ Sci Pollut Res Int 21:5879-5888. https://doi.org/10.1007/s11356-014-2529-0
16. Kergaravat SV, Pividori MI, Hernandez SR (2012) Evaluation of seven cosubstrates in the quantification of horseradish peroxidase enzyme by square wave voltammetry. Talanta 88:468-476. https://doi.org/10.1016/j.talanta.2011.11.016
17. Lin Z, Xiao Y, Yin YQ, Hu WL, Liu W, Yang H (2014) Facile Synthesis of Enzyme-Inorganic Hybrid Nanoflowers and its Application as a Colorimetric Platform for Visual Detection of Hydrogen Peroxide and Phenol. ACS Appl Mater Inter. https://doi.org/10.1021/am502757e
18. Liu K, Nasrallah J, Chen L, Huang L, Ni Y (2015) Preparation of CNC-dispersed Fe_3O_4 nanoparticles and their application in conductive paper. Carbohydr Polym 126:175-178. https://doi.org/10.1016/j.carbpol.2015.03.009
19. Low LE, Tey BT, Ong BH, Tang SY (2018) Unravelling pH-responsive behaviour of Fe_3O_4@CNCs-stabilized Pickering emulsions under the influence of magnetic field. Polymer 141:93-101. https://doi.org/10.1016/j.polymer.2018.03.001
20. Mei LP, Feng JJ, Wu L, Zhou JY, Chen JR, Wang AJ (2015) Novel phenol biosensor based on laccase immobilized on reduced graphene oxide supported palladium-copper alloyed nanocages. Biosens Bioelectron 74:347-352. https://doi.org/10.1016/j.bios.2015.06.060
21. Meng J, Shi C, Wei B, Yu W, Deng C, Zhang X (2011) Preparation of Fe_3O_4@C@PANI magnetic microspheres for the extraction and analysis of phenolic compounds in water samples by gas chromatography-mass spectrometry. J Chromatogr A 1218:2841-2847. https://doi.org/10.1016/j.chroma.2011.03.044
22. Mitra R, Saha A (2016) Reduced Graphene Oxide Based “Turn-On” Fluorescence Sensor for Highly Reproducible and Sensitive Detection of Small Organic Pollutants. ACS Sustain Chem Eng 5:604-615. https://doi.org/10.1021/acssuschemeng.6b01971
23. Niu K, Gao J, Wu L, Lu X, Chen J (2021) Nitrogen-Doped Graphdiyne as a Robust Electrochemical Biosensing Platform for Ultrasensitive Detection of Environmental Pollutants. Anal Chem:34110153. https://doi.org/10.1021/acs.analchem.1c01800
24. Qiao F, Chen L, Li X, Li L, Ai S (2014) Peroxidase-like activity of manganese selenide nanoparticles and its analytical application for visual detection of hydrogen peroxide and glucose. Sensor Actuat B-Chem 193:255-262. https://doi.org/10.1016/j.snb.2013.11.108

25. Vetr F, Moradi-Shoeili Z, Özkar S (2018) Oxidation of o-phenylenediamine to 2,3-diaminophenazine in the presence of cubic ferrites MFe_2O_4(M = Mn, Co, Ni, Zn) and the application in colorimetric detection of H_2O_2. Appl Organomet Chem 32. https://doi.org/10.1002/aoc.4465
26. Wu S, Guo D, Xu X, Pan J, Niu X (2020) Colorimetric quantification and discrimination of phenolic pollutants based on peroxidase-like Fe_3O_4 nanoparticles. Sensor Actuat B-Chem 303:127225. https://doi.org/10.1016/j.snb.2019.127225
27. Wu Y et al. (2019) Determination of practical application potential of highly stable UiO-66-AO in Eu(III) elimination investigated by macroscopic and spectroscopic techniques. Chem Eng J 365:249-258. https://doi.org/10.1016/j.cej.2019.02.053
28. Wu Y et al. (2017) Metal-organic framework coated Fe_3O_4 magnetic nanoparticles with peroxidase-like activity for colorimetric sensing of cholesterol. Sensor Actuat B-Chem 249:195-202. https://doi.org/10.1016/j.snb.2017.03.145
29. Xiong R, Lu C, Wang Y, Zhou Z, Zhang X (2013) Nanofibrillated cellulose as the support and reductant for the facile synthesis of Fe_3O_4/Ag nanocomposites with catalytic and antibacterial activity. J Mater Chem A 1:14910. https://doi.org/10.1039/c3ta13314a
30. Yang D, Li Q, Tammina SK, Gao Z, Yang Y (2020) Cu-CDs/H_2O_2 system with peroxidase-like activities at neutral pH for the co-catalytic oxidation of o-phenylenediamine and inhibition of catalytic activity by Cr(III). Sensor Actuat B-Chem 319:128273. https://doi.org/10.1016/j.snb.2020.128273
31. Yang J, Zhang F, Lu H, Hong X, Jiang H, Wu Y, Li Y (2015) Hollow Zn/Co ZIF Particles Derived from Core-Shell ZIF-67@ZIF-8 as Selective Catalyst for the Semi-Hydrogenation of Acetylene. Angew Chem Int Ed Engl 54:10889-10893. https://doi.org/10.1002/anie.201504242
32. Ye Y, Kong T, Yu X, Wu Y, Zhang K, Wang X (2012) Enhanced nonenzymatic hydrogen peroxide sensing with reduced graphene oxide/ferroferric oxide nanocomposites. Talanta 89:417-421. https://doi.org/10.1016/j.talanta.2011.12.054
33. Zeng Z, Tian L, Li Z, Jia L, Zhang X, Xia M, Hu Y (2015) Whole-cell method for phenol detection based on the color reaction of phenol with 4-aminoantipyrine catalyzed by CotA laccase on endospore surfaces. Biosens Bioelectron 69:162-166. https://doi.org/10.1016/j.bios.2015.02.032
34. Zheng HQ et al. (2018) MOF-808: A Metal-Organic Framework with Intrinsic Peroxidase-Like Catalytic Activity at Neutral pH for Colorimetric Biosensing. Inorg Chem 57:9096-9104. https://doi.org/10.1021/acs.inorgchem.8b01097
35. Zheng J, Cheng C, Fang W, Chen C, Yan R, Huai H, Wang C (2014) Surfactant-free synthesis of a Fe_3O_4@ZIF-8 core-shell heterostructure for adsorption of methylene blue. CrystEngComm 16. https://doi.org/10.1039/c3ce42648c

Figures

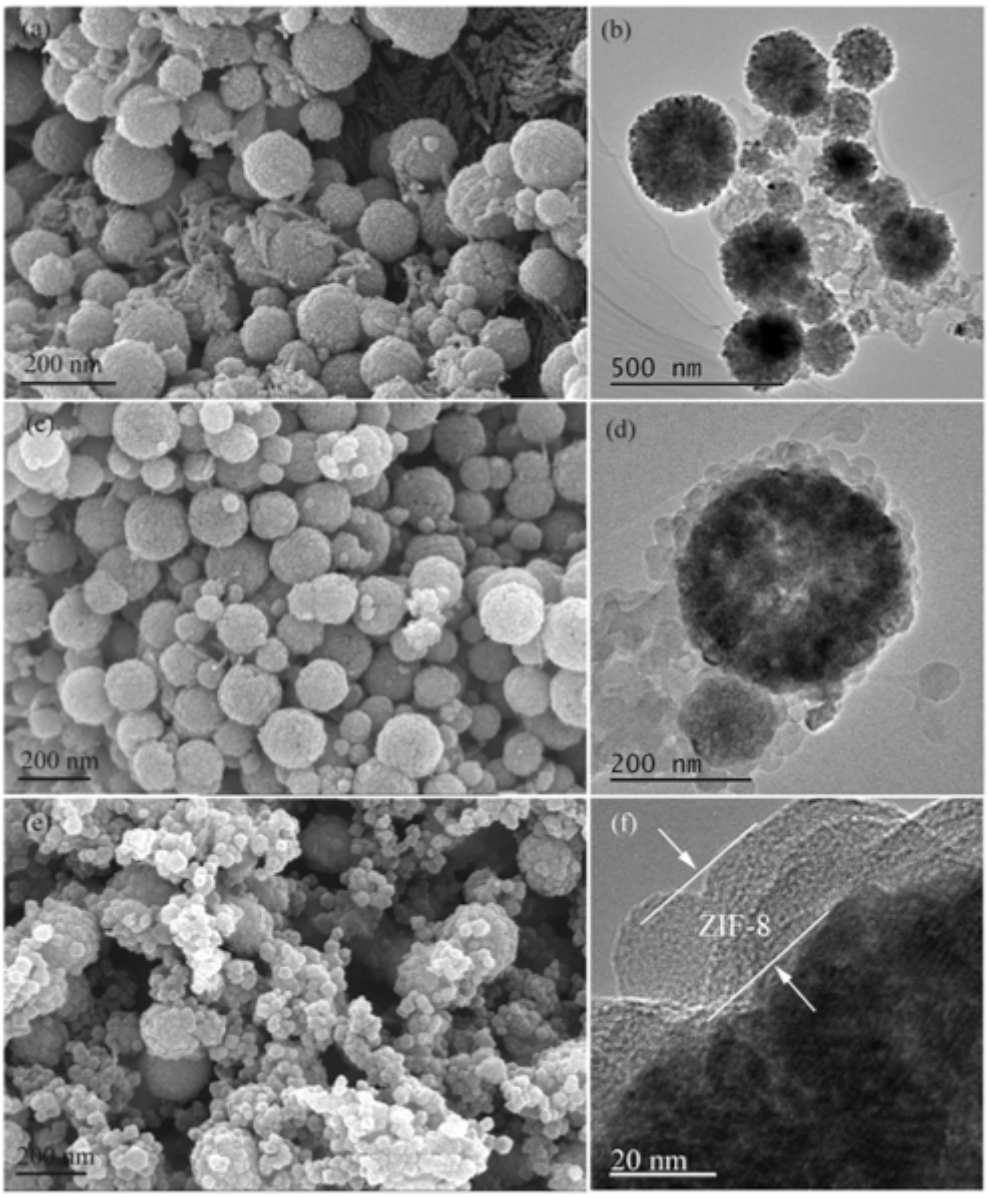

Figure 1

SEM image of (a) Fe3O4/CNC, (c) Fe3O4/CNC/TA, (e) Fe3O4/CNC@ZIF-8; TEM image of (b) Fe3O4/CNC, (d) and (f) Fe3O4/CNC@ZIF-8

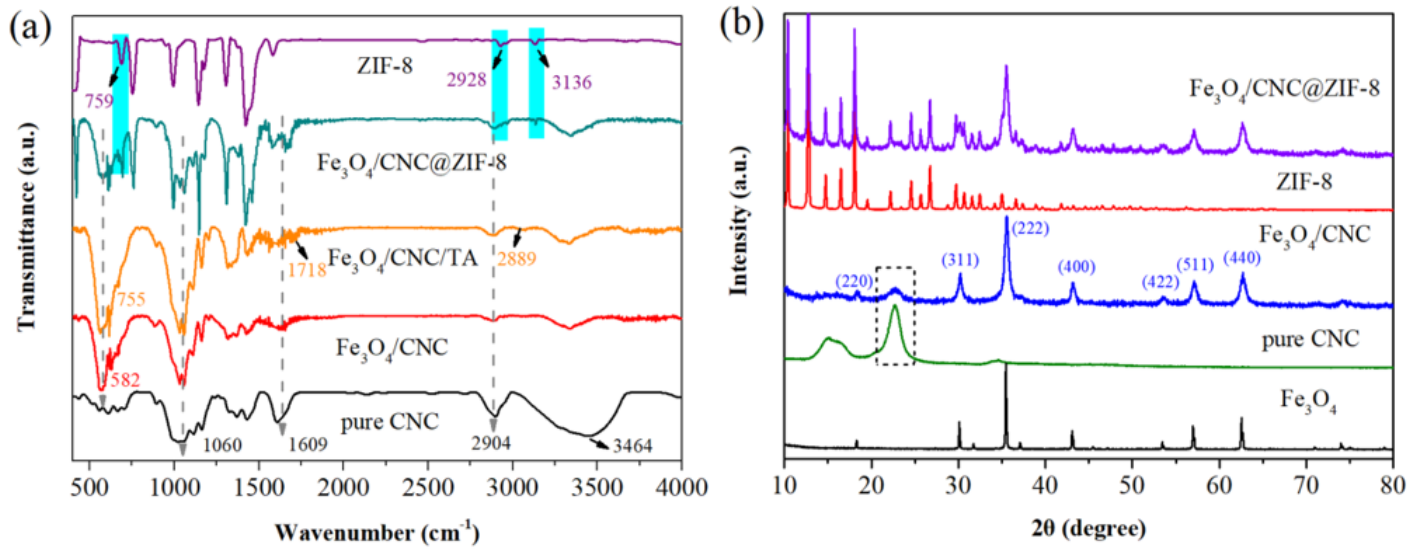

Figure 2

FT-IR spectrum (a) of pure CNC, Fe3O4/CNC, Fe3O4/CNC/TA, Fe3O4/CNC@ZIF-8 and ZIF-8; XRD spectra (b) Fe3O4, pure CNC, Fe3O4/CNC, ZIF-8 and Fe3O4/CNC@ZIF-8

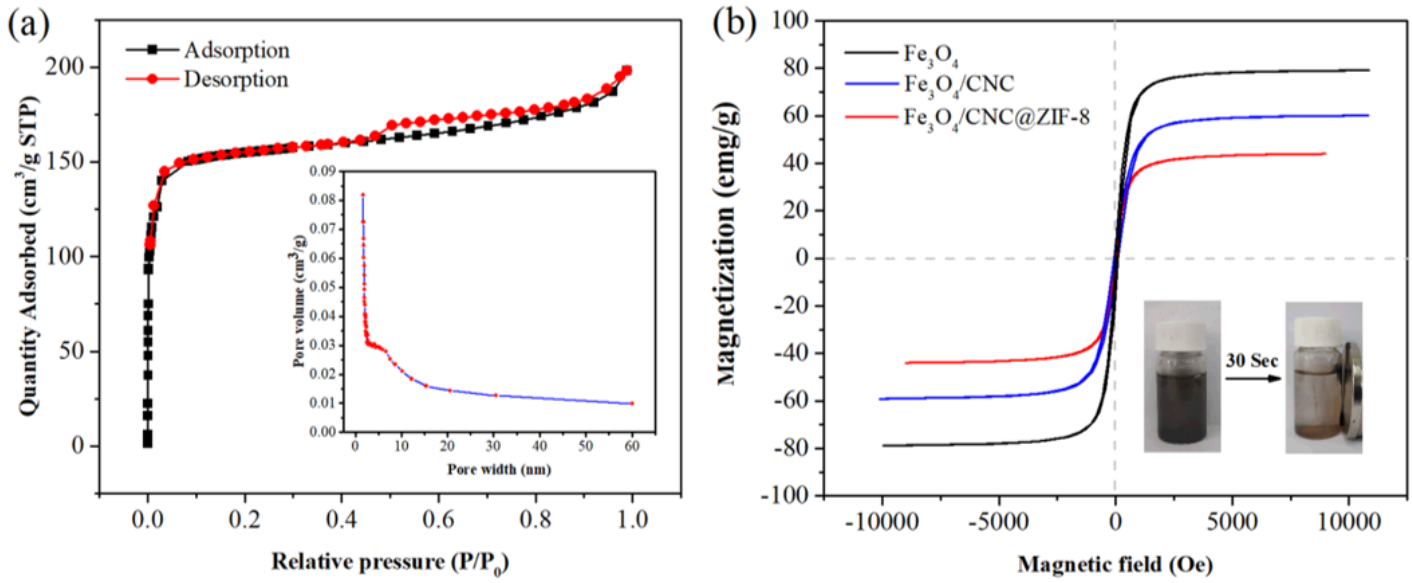

Figure 3

(a) N2 absorption-desorption isotherms of Fe3O4/CNC@ZIF-8; (b) hysteresis loops of Fe3O4, Fe3O4/CNC and Fe3O4/CNC@ZIF-8

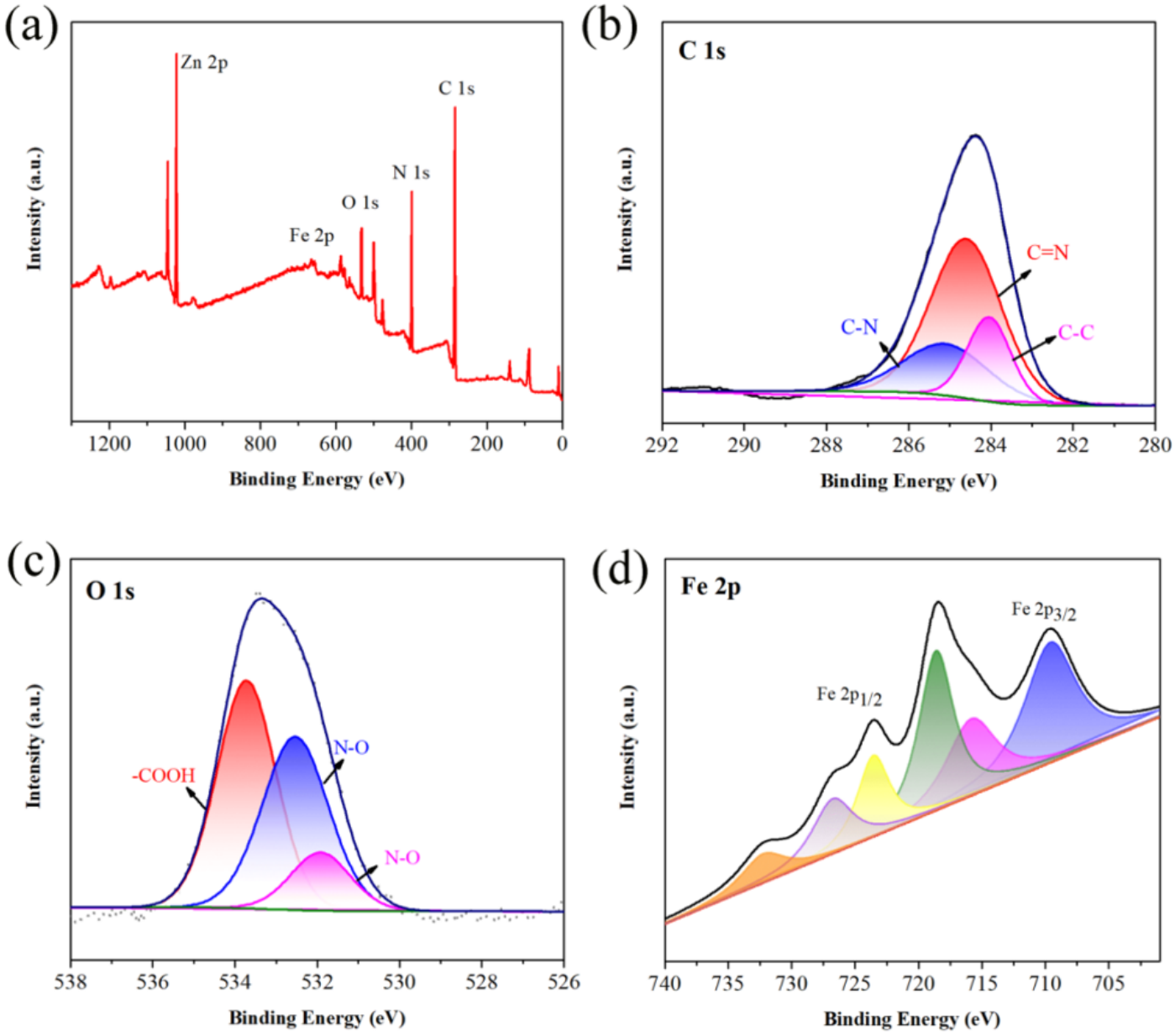

Figure 4

(a) XPS spectra of Fe3O4/CNC@ZIF-8; the high-resolution XPS spectrums for C 1s (b), O 1s (c) and Fe 2p (d)

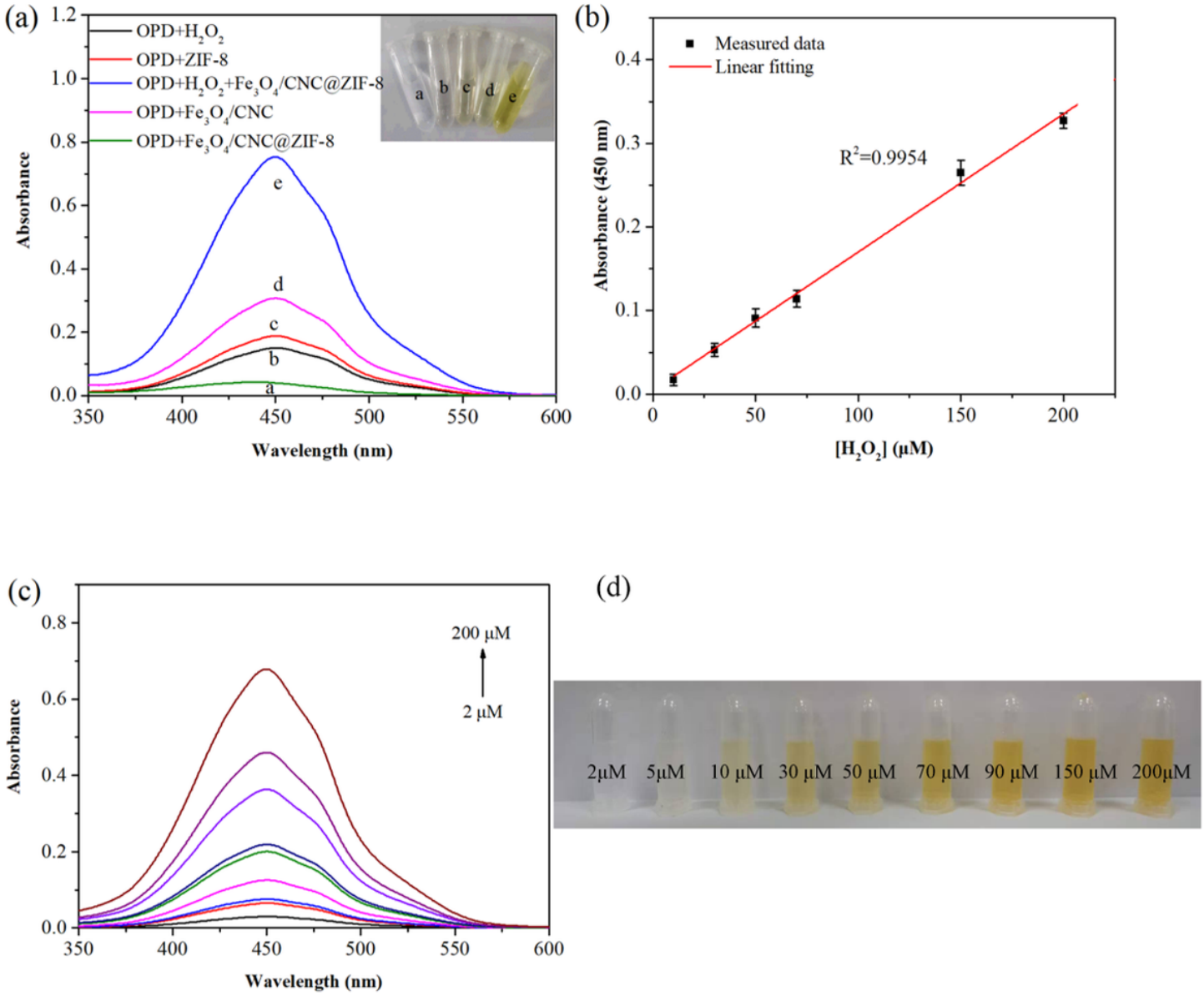

Figure 5

(a) The UV-vis spectra of different systems; (b) UV-vis absorption spectra of OPD solutions containing Fe3O4/CNC@ZIF-8 upon the addition of 2-200 μM H2O2; (c) the plot of A450 versus H2O2 concentration; (d) colorimetric change of OPD solutions containing Fe3O4/CNC@ZIF-8 upon the addition of 2-200 μM H2O2

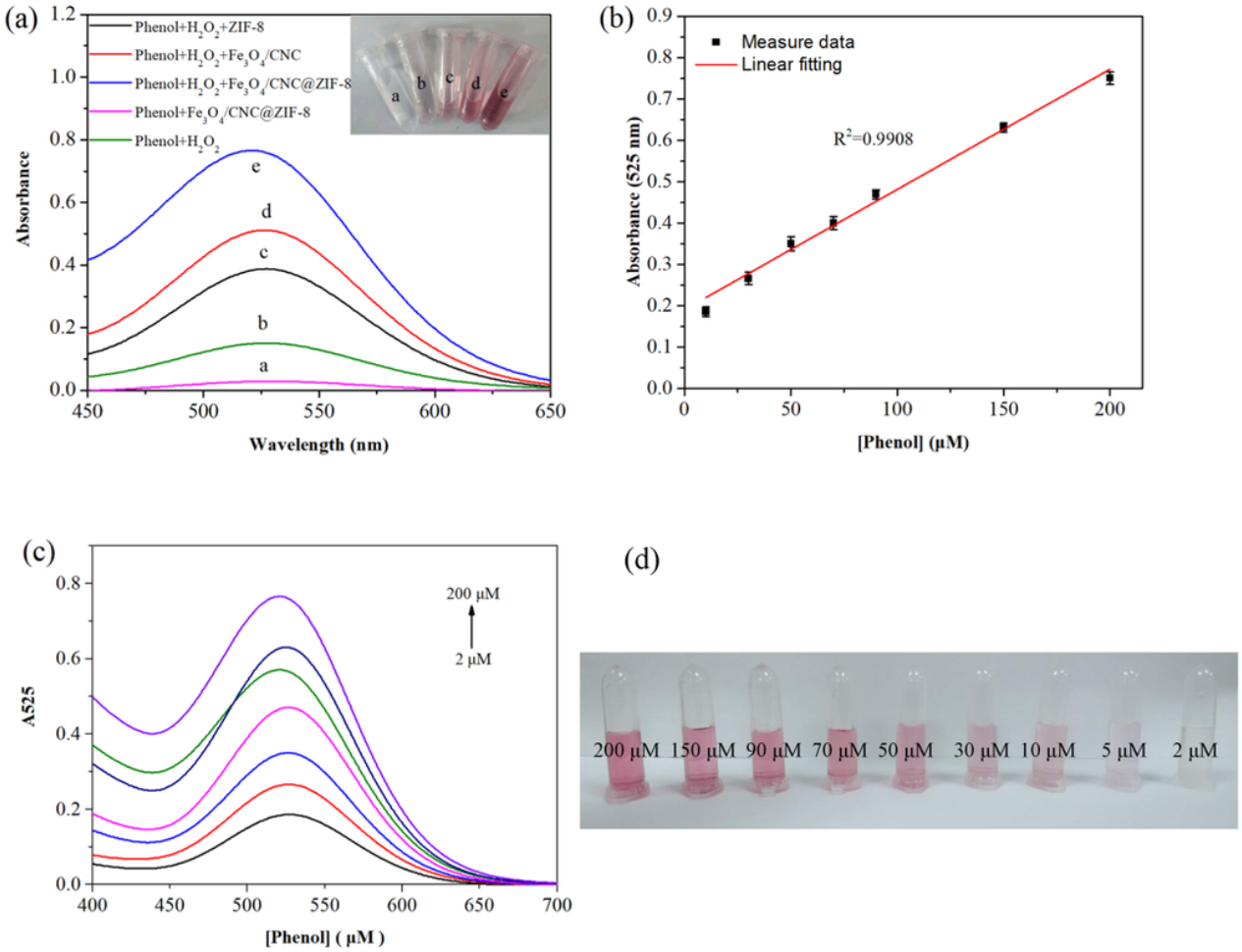

Figure 6

(a) The UV-vis spectra of different systems; (b) UV-vis absorption spectra of 4-AAP solutions containing Fe3O4/CNC@ZIF-8 upon the addition of 2-200 μM phenol; (c) the plot of A 525 versus phenol concentration; (d) colorimetric change of 4-AAP solutions containing Co3O4/CDM upon the addition of 2-200 μM phenol

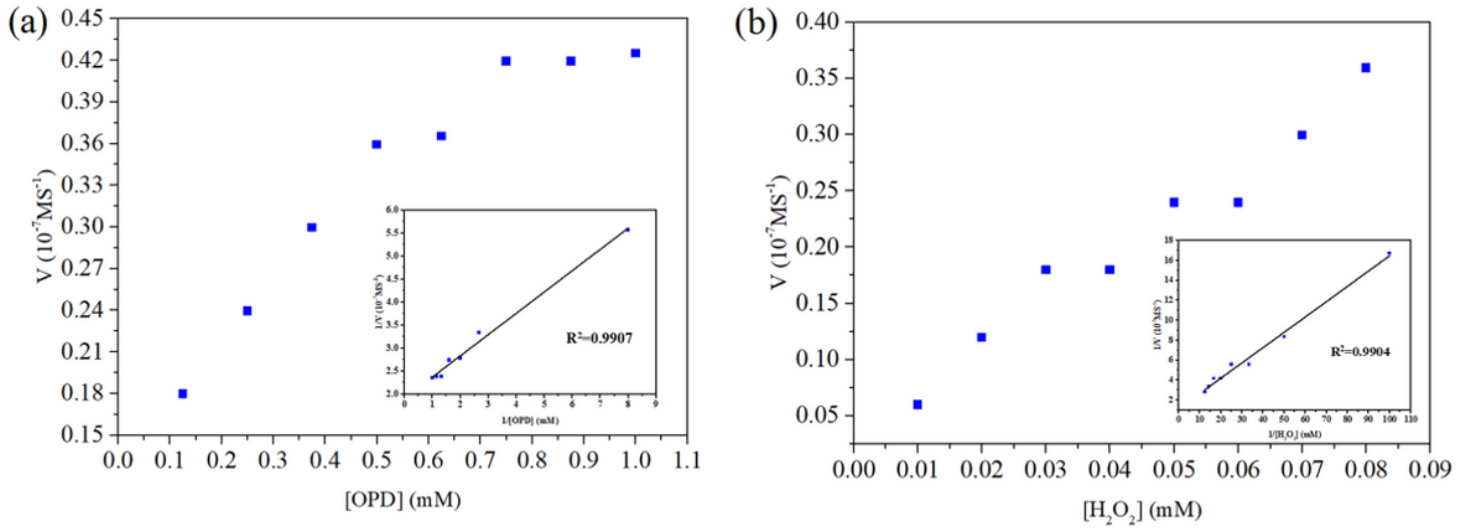

Figure 7

Steady-state kinetic assay of Fe3O4/CNC@ZIF-8; (a) Variation of TMB concentration at constant H2O2 concentration; (b) Variation of H2O2 concentration at constant TMB concentration; The corresponding Lineweaver-Burk plots of the double reciprocal of Michaelis Menten equation are shown in the inset

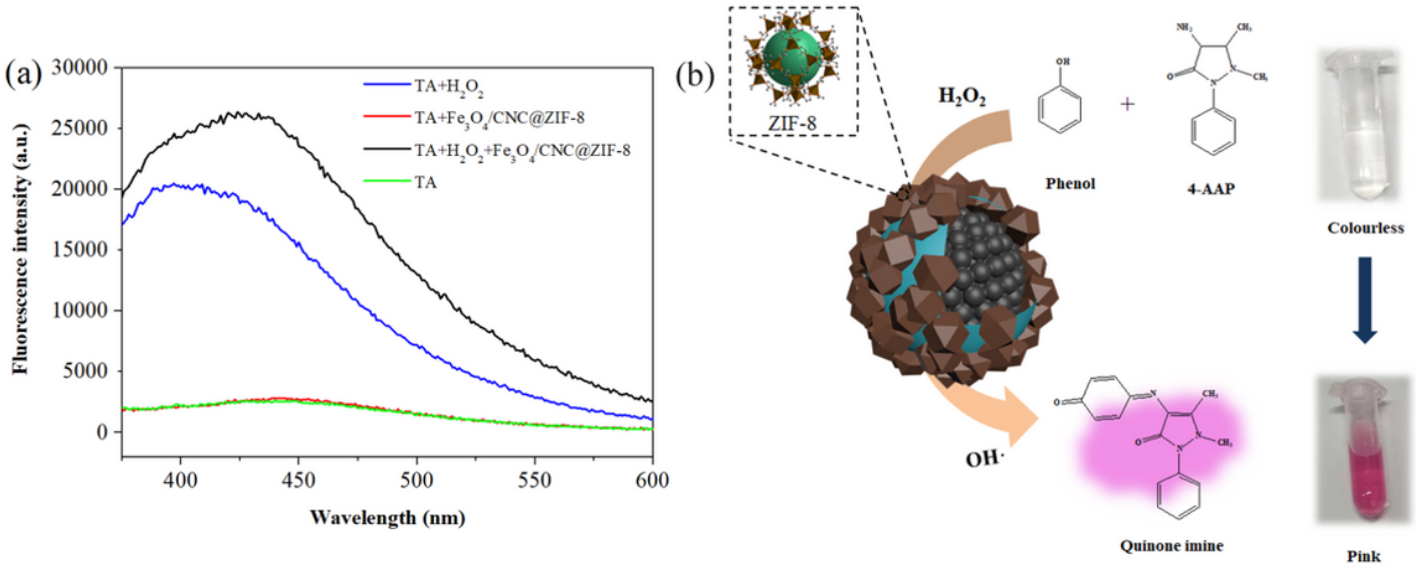

Figure 8

(a) The fluorescence spectra of different systems; (b) Catalytic mechanism of Fe3O4/CNC@ZIF-8

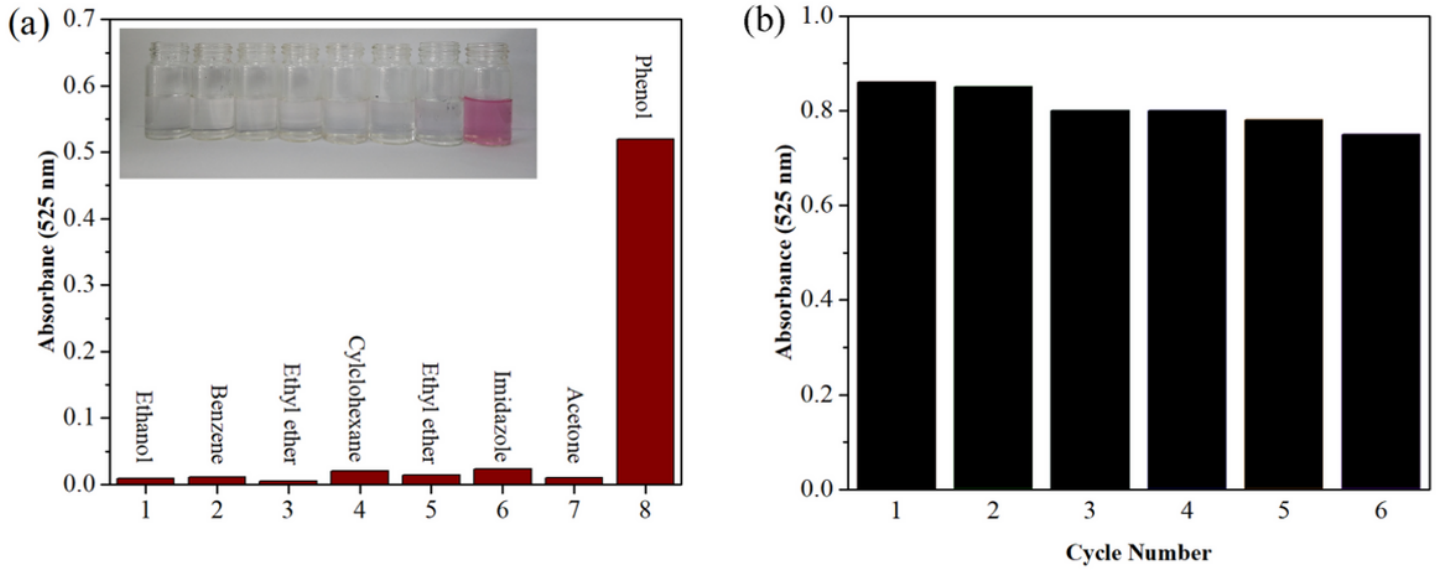

Figure 9

(a) Value at 525 nm of the solutions containing 70 μM phenol or various species; (b) Value at 525 nm of phenol after each cycle

Supplementary Files

This is a list of supplementary files associated with this preprint. Click to download.

- schema.png
- SI.docx